

Investigation of the Structural and Magnetic Properties of the Light Rare Earth Elements and Their Intermetallic Compounds*

D. C. Creagh

Department of Physics, University College,
University of New South Wales, Australian Defence Force Academy,
Campbell, A.C.T. 2600, Australia.

Abstract

The experimental requirements for the investigation of the structural and magnetic properties of the light rare earth elements and their intermetallic compounds at synchrotron radiation sources are discussed. Experimental techniques considered include X-ray topography, energy dispersive X-ray diffraction and X-ray powder diffraction.

1. Introduction

The unique properties of the electromagnetic radiation produced by accelerating electrons and positrons in synchrotrons and storage rings have been discussed in many books and review articles (see, for example, Teo and Joy 1981; Bianconi *et al.* 1983; Hosoya *et al.* 1986). Some of the many topics which are studied at synchrotron radiation facilities, and the techniques used for that study, are shown in Table 1. Subjects studied at synchrotron facilities cover the A to Z of science, archaeology to zoology, and it is not surprising therefore that there is great diversity in the experimental requirements for these very different study areas.

It is not possible to address such a broad issue in the limited space available here. Therefore my discussion will be limited to the study of the structural and magnetic properties of the light rare earth metals and their alloys, discussing first the properties of synchrotron radiation, then the structural and magnetic properties of this class of materials. In doing so I shall discuss the instrumentation required to enable the appropriate experiments to be mounted at a synchrotron radiation facility, describing in particular the monochromator systems to be used to provide the necessary conditions for studies of the structural and magnetic properties of magnetic materials.

2. Synchrotron Radiation and Its Properties

In synchrotron particle accelerators and storage rings the particles undergoing acceleration are electrons or positrons or both electrons and positrons circulating in

* Paper presented at the International Symposium on X-ray Powder Diffractometry, held at Fremantle, Australia, 20-23 August 1987.

Table 1. Techniques used in the study of subjects at synchrotron radiation sources

Subjects	X-ray diffr.	Small angle X-ray diffr.	Topography	EXAFS XANES
Atomic physics				×
Surface studies	×		×	×
Photochemistry	×	×		×
Elect. prop. of solids	×			
Phase changes	×	×	×	
Defects in solids	×	×	×	
Geology	×		×	
Chemistry	×	×		
Biology	×	×		

opposite senses. The radiation emitted is highly intense with a spectral brilliance more than 10^4 times as intense as the radiation emitted from a conventional fine focus X-ray tube. This radiation is emitted over a wide spectral range from a short wavelength cut-off of less than 1 Å, determined by the energy of the particle and the radius of curvature of the orbit

$$\lambda_c = 5.6B/E^3 \quad (1)$$

where B is the magnetic induction in Tesla and E is the energy in GeV, to the visible region. In practice, however, this upper cut-off is determined by the nature of the vacuum system and equipment interface. Note that the variation of intensity with wavelength is smooth. In contrast a conventional sealed tube emits bremsstrahlung over a much more restricted wavelength range, and its emission spectrum contains the characteristic radiation of the materials from which the target is constructed. A comparison of the spectral emission by synchrotron and conventional sources is given in Fig. 1*a*.

The fact that the particles accelerated by a synchrotron radiation source are moving with relativistic velocities means that the dipolar radiation field is heavily distorted in a direction tangential to the orbit. This has two important results:

- (i) the radiation emitted is very highly collimated, with typical beam divergences being less than 50 seconds of arc; and
- (ii) the radiation is highly polarised, being 100% linearly polarised in the plane of the orbit, as shown in Fig. 1*b*.

In contrast the radiation emitted from conventional sources is uncollimated, and circularly or elliptically polarised, depending somewhat on the construction of the X-ray tube and the nature of the target–equipment interface.

Because the charged particles are accelerated in bunches, synchrotron radiation sources are pulsed with a duty cycle of typically 0.01. In contrast conventional radiation sources have a steady radiation output. The time structure of the synchrotron can be used to study rapidly varying phenomena stroboscopically.

The problem to be addressed here is: given access to a synchrotron radiation beam line, what experiments can we perform to solve some of the structural and magnetic properties of the light rare earth elements and their alloys? To proceed further with this discussion it is necessary to describe briefly the crystallography of these materials.

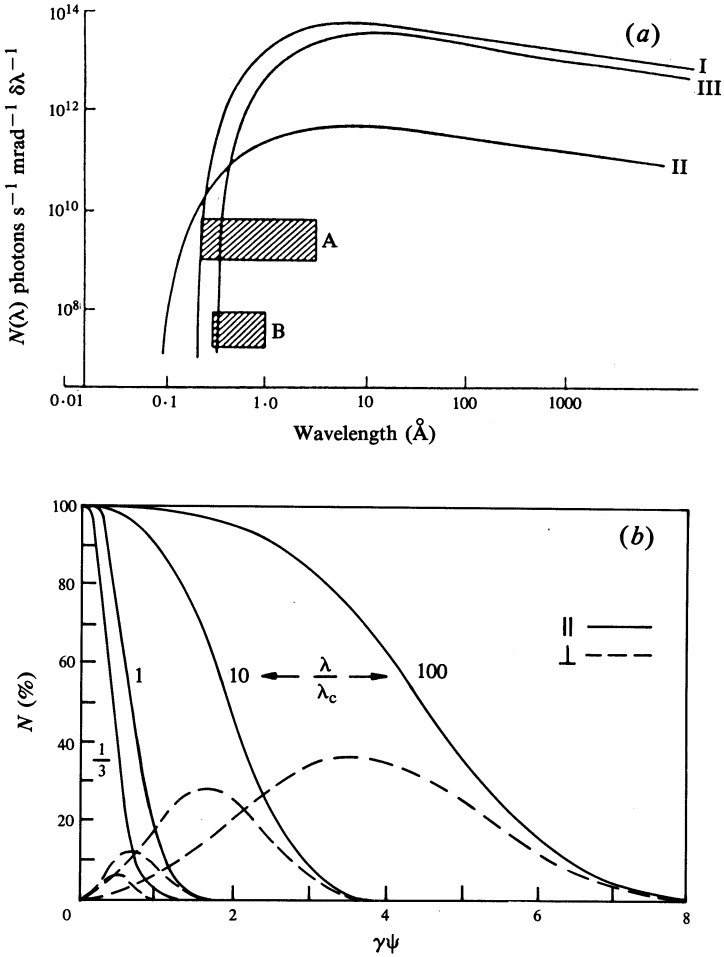


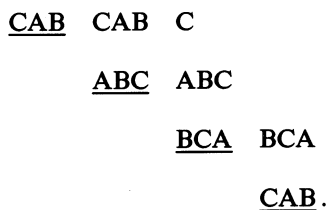
Fig. 1. (a) Spectral output from several synchrotrons and storage rings: curve I, the storage ring DORIS at Hamburg; curve II, the synchrotron NINA at Daresbury Laboratory; and curve III, the storage ring at Daresbury Laboratory. The rectangle A covers the range within which characteristic line sources are available, while B covers the bremsstrahlung from a 60 kW rotating anode X-ray tube. (b) Vertical angular distribution of parallel and perpendicular polarisation components shown for three values of λ/λ_c as a function of $\gamma\psi$, where $\gamma = E/mc^2$, ψ is the vertical angle (rad), and $\lambda_c = 186.4/BE^2$; with B the bending field and E the photon energy.

3. Crystallography of the Light Rare Earths and Their Alloys

As Coles (1980) and Creagh (1985) have pointed out most of the light rare earth metals and alloys exhibit both complicated magnetic properties [see e.g. Fig. 3 in Section 4 which shows a magnetisation curve for terbium taken from McKenna *et al.* (1980)] and also crystallographic structures [either doubly hexagonal close packed (dhcp) or samarium (Sm) structures]. Both these structures may be regarded as periodic variations of the hexagonal close packed (hcp) or face-centred cubic (fcc) structures.

It is well known that for some of the transition metals (e.g. cobalt) the hcp stacking sequence (ABABAB...) and the fcc sequence (ABCABC...) have very similar free energies, so that there can exist in equilibrium in fcc cobalt a substantial volume of material in the hcp configuration (Creagh *et al.* 1975). A similar situation has been shown to exist for the Laves phase intermetallic compounds $GdFe_2$, $GdCo_2$ and $GdNi_2$ where these errors in stacking, stacking faults, were shown to be equivalent to one complete layer for every five stacked layers (Creagh and Ayling 1978).

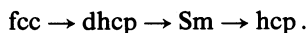
The Sm structure may be regarded as a fcc structure with a positive stacking fault every third layer:



Slightly different complicated sequences in the stacking of fcc can produce the dhcp structure. Such long period stacking fault structures have been shown to exist by Van Vucht and Buschow (1965) for the class of intermetallic compounds RAI_3 , where R is a rare earth. When the rare earth atom is changed to one of higher atomic number, the crystal structure changes:



Here X is a 15 layer structure corresponding to a dhcp structure with a stacking fault every fifth layer. For the pure rare earth metals the transition is



The crystal structures are determined by the requirement that the cohesive energy be a minimum. The cohesive energy is determined for the most part by the metallic binding term, which is in turn determined by Coulomb interactions between electrons. For these metals the f electrons have no effect on the transition since they are highly localised in character. The occupied s (actually s-p hybrid) states lie close to the Brillouin zone centre and are therefore insensitive to crystal structure. However, the occupied d states lie near the Brillouin zone surface and strongly influence the crystal structure. The transitions are directly linked to the increase in the number of d electrons from 1.5 to 2.5.

Another term of significance (and one which is usually neglected) is the interaction between electron spins (and indeed other more indirect magnetic interactions). I shall not discuss in detail these effects, simply noting that the magnetic term has an influence on the crystal structure of these materials, and that the inverse can also be true, i.e. defects in crystal structure can influence magnetic properties.

It must also be stressed that there are two types of faulting in fcc structures:

- (i) deformation faulting, for which the stacking sequence is $ABC|BCABC$, and the probability for formation of which is usually designated by α ; and
- (ii) growth faulting (or twin faulting), for which the stacking sequence is $ABC|BAC$, and the probability for formation of which is designated by β .

The probabilities α and β for stacking fault formation are related to both the position and width of X-ray diffraction profiles (see e.g. Warren 1969).

4. Possible Experiments using Synchrotron Radiation Sources

In this section I shall describe experiments which involve equipment of increasing complexity, my aim being to stress that effective experiments can be performed with quite simple equipment.

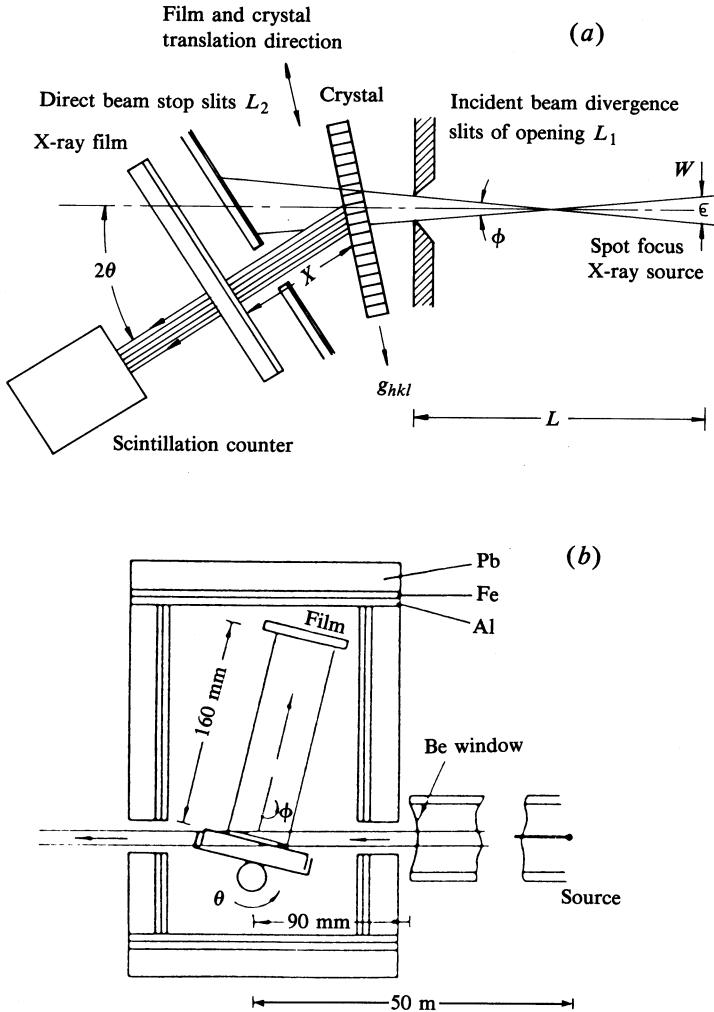


Fig. 2. (a) Lang technique for X-ray topography. (b) Continuous radiation technique for use with synchrotron radiation.

(a) Using the Spectral Range and Intensity: X-ray Topography

Diffracted beam X-ray topography has long been a routine tool for the study of both defects and magnetic domains in crystals (Tanner 1977). When used with conventional X-ray sources the X-ray beam is collimated by slits and the crystal

under examination set to reflect the chosen diffracted beam (diffraction vector q). A film is placed normal to the diffracted beam, and behind a selecting slit which remains stationary during an exposure. In the conventional Lang (1959) approach (see Fig. 2a) an exposure is carried out by traversing both the crystal and film across the X-ray beam. The characteristic radiation from the source is used and (usually) the crystal is set to select only the $K\alpha_1$ radiation. The presence of dislocations, stacking faults and other defects are observed through the strain fields they cause on the lattice, and the criterion for visibility is that

$$g \cdot b = 0,$$

where b is the Burgers vector of the dislocation. Similarly magnetic domains are observed because of the strain fields caused by magnetostriction and a variety of visibility criteria exist, the simplest of which is

$$g \cdot \Delta m = 0,$$

where Δm is the change in magnetisation between neighbouring domains.

In contrast the white beam topography technique used for topographic studies at synchrotron radiation sources is both simple to use and inexpensive to mount. It makes use of the fact that the synchrotron beam is already very highly collimated, has a large size (usually 10 mm diameter) and spans a broad range of photon energies. The technique is similar to the Laue method used for specimen orientation, and is shown schematically in Fig. 2b. Each Laue spot contains information concerning the defect state of the crystal, and since many spots exist, each with a different g , the identification of the orientation of the d domain walls is rapid and easy. Placing the sample in a cryostat enables the variation of magnetisation to be plotted as a function of temperature. However, this may reduce significantly the number of diffracted beams which can be observed.

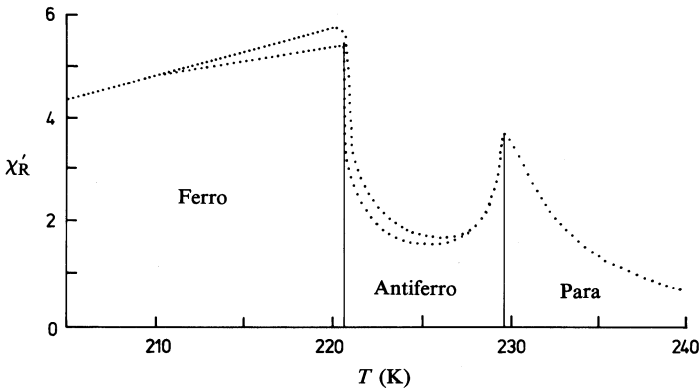


Fig. 3. Real part of the magnetic susceptibility of terbium as a function of temperature. [From McKenna *et al.* (1980).]

The rare earths exhibit complicated magnetisation properties when the temperature is varied. Fig. 3 shows the results of an AC susceptibility experiment performed on a single crystal of terbium. At low temperatures it is ferromagnetic with a Curie temperature of 221 K. A region exhibiting antiferromagnetism exists at higher temperatures. The Néel temperature is 229 K.

Access to a synchrotron radiation source considerably enhances the possibility of studying domain formation in magnetic materials. If the specimen were to be placed in a solenoid and excited, for example by an AC magnetic field, it would be possible to take stroboscopic topographs of the specimen at different times during the AC cycle, thus mapping the motion of domain walls (Miltat 1978), and demonstrating the influence which crystal defects, grain boundaries and crystal strain have on domain wall propagation. If a tensile stage were to be added the influence of external stress on domain wall motion could be investigated (Clark and Tanner 1980). If the film were to be replaced by an X-ray photo-optical photon converter it is possible to image this output onto a TV camera so that these motions can be seen directly (Chikawa *et al.* 1986).

None of these experiments outlined needs expensive or complicated equipment to produce acceptable results: merely access to the high intensity, spectrally broad-band, highly collimated output from a synchrotron radiation source.

(b) Energy Dispersive X-ray Diffraction (EDXRD)

In the previous subsection the sample was a single crystal or a polycrystal, for which the subgrains are relatively large, and the detector was a film. For specimens in the form of fine grained polycrystal powders or amorphous alloys, a simple modification can be made to enable the system to be used as a diffractometer, namely, the sample may be mounted to intercept the primary beam and a solid state detector [Si(Li) or intrinsic germanium] placed at a known angle $2\theta_0$ to the incident beam. The detector output is taken to an appropriate multichannel analyser.

The white collimated X-ray beam is scattered by the sample through a fixed angle $2\theta_0$ and the energy distribution of the scattered (and fluorescent) photons is analysed by the solid state detector system. The modulus of the scattering vector is given by

$$|q| = (6.2/2\pi)E \sin \theta_0,$$

where q is expressed in \AA^{-1} and the photon energy E in keV.

For a detector with a calibrated response function it is possible to determine the scattering function $S(q)$ which describes the structure in momentum space. Measurement of the intensities of the fluorescent radiation enables the composition of the sample to be determined (see e.g. Bertin 1975).

The fixed geometry of the diffractometer is especially useful for studies of samples in special environments (e.g. high pressure and/or low or high temperature) because only one outlet window is required for the diffracted beam. The highly intense incident photon beam enables short exposure times and allows following structural changes on a time-scale measured in seconds (Egami 1978).

Measurements of the scattering function $S(q)$ are made simultaneously for a wide range of q , but the resolution is significantly worse than that obtainable from conventional X-ray diffractometers. Nevertheless, EDXRD has a very important role to play and may be undertaken with very little expenditure on experimental apparatus.

(c) Single Wavelength Techniques

Since the synchrotron radiation has a broad spectral range it is necessary to introduce some form of monochromator into the beam if experiments are to be undertaken at a particular wavelength. Such a monochromator is ideally able to be

tuned over a comparatively wide wavelength range (say 0.5 to 2.5 Å). It is not possible here to discuss all the possible monochromator designs which are in use; rather I shall describe briefly the principles of operation of two of the more simple monochromators which are to be used for the 'Photon Factory'.

For the principles of operation of symmetrically cut multiple element monochromator systems see Hart and Rodrigues (1978, 1979) and Hart *et al.* (1984). For asymmetrically cut monochromator systems the work of Renrigger (1967) has been extended substantially by Kikuta and Kohra (1968, 1970), Matsushita *et al.* (1971) and Hashizume and Kohra (1971).

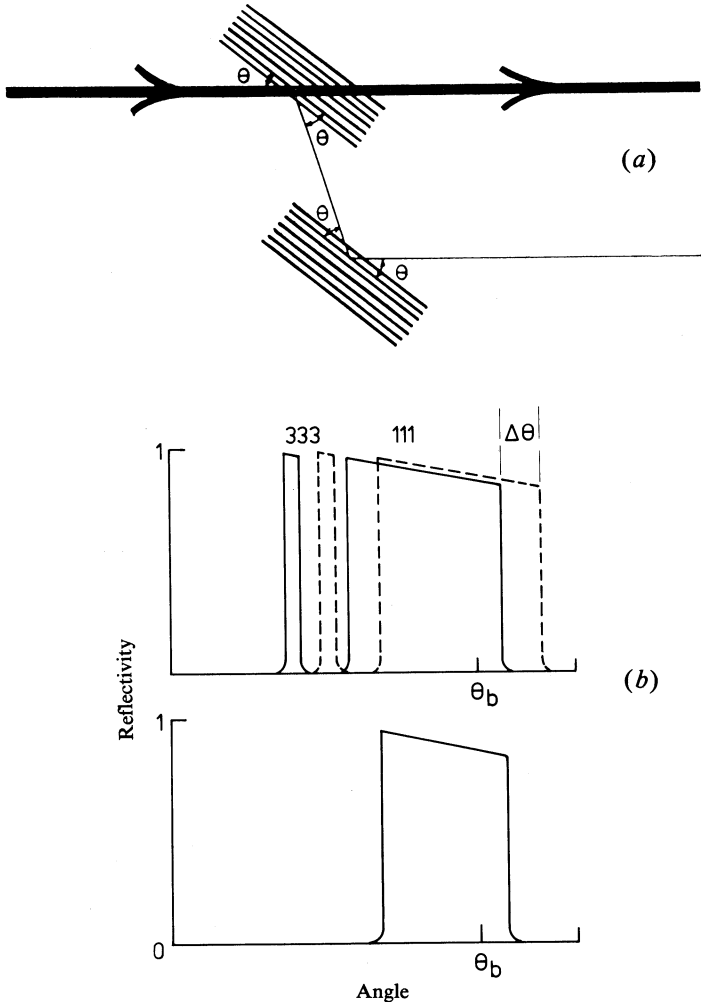


Fig. 4. (a) Schematic representation of a double crystal monochromator. For each crystal the Bragg condition must be satisfied for reflection to occur. (b) Reflectivity curves for silicon (111).

(d) Independent Element Double Crystal Monochromators

The simplest form of multiple element monochromator consists of two plane elements cut from defect-free single crystals parallel to the appropriate Bragg reflecting

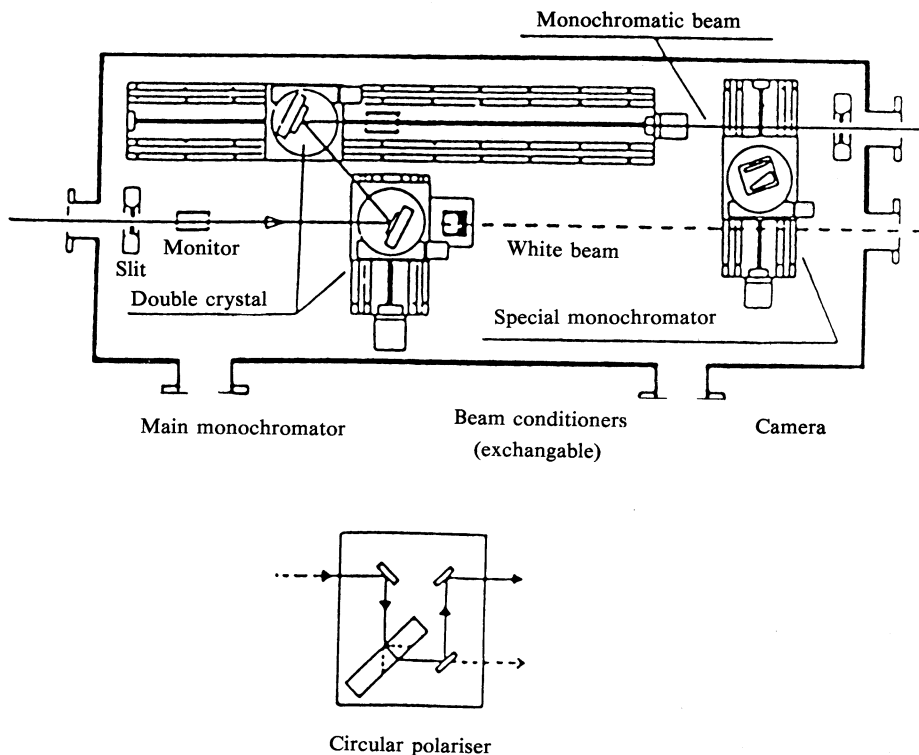


Fig. 5. Schematic representation of the monochromator system proposed for the Photon Factory. In the evacuated monochromator chamber are facilities to enable the use of a double crystal monochromator system, an asymmetric-symmetric monochromator system, a white beam, and a circular polarising monochromator.

plane. One element is situated on the axis of a rotary table (θ -axis) mounted on a linear slide and the other on a rotary table mounted on a linear slide which can move in a direction normal to the first slide (see Figs 4a and 5). The axes are constructed with an upper stage for which piezoelectric elements drive lever arms to enable the setting of the monochromator elements to better than $0.01''$. This is necessary since for example the width of the 422 rocking curve for a single reflection from silicon is only $3''$ at 1.54 \AA .

This configuration enables the monochromator to be tuned over a wide wavelength range whilst keeping the spatial separation of the incident and exit beams constant. This latter property is essential if constant repositioning of the sample is to be avoided.

In the case where both elements of the monochromator lie parallel to one another the Bragg condition

$$2d_{hkl} \sin \theta = n\lambda$$

is fulfilled for not only the fundamental ($n = 1$) but for all harmonics allowed by the crystal structure. This can be a source of problems because of the range of wavelengths incident upon the monochromator. Harmonics up to $n = 16$ have been observed. To produce only the fundamental it is necessary to displace one of the reflecting crystals slightly from the exact Bragg condition. Since the harmonic reflections have widths $\sim F_n/n^2 F_0$, where F_n is the geometrical structure factor of

the n th reflection and F_0 is the geometrical structure factor for the fundamental, and both are located at positions different from the exact Bragg condition of the fundamental because of refractive index effects (see Fig. 4*b*), it is necessary only to set an offset of $\Delta\theta \geq 0.25''$ on one of the crystals in order to ensure that the Bragg reflection of the n th reflection in the first element does not satisfy the Bragg condition of the n th reflection in the second element.

What has been said for simple symmetrical single element devices holds true also for multiply reflecting grooved single crystal devices, as Bonse and Hart (1965) have shown. Hart *et al.* (1984) have described in some detail the construction and properties of monolithic single crystal monochromator systems.

Reverting to the simple two crystal–two reflection monochromator system, another option that exists for the elimination of harmonics is cutting one of the crystals such that its surface is at an angle α to the Bragg reflecting planes. By an appropriate choice of α for a particular wavelength it is possible to narrow the range of Bragg reflection, eliminate the passage of harmonics, and reduce the spatial dimensions of the beam. For asymmetric diffraction from a surface making an angle α with the Bragg plane, the angular widths of acceptance ω_i and emergence ω_e are related to the symmetric halfwidth by

$$\omega_i = \omega_s / b^{\frac{1}{2}}; \quad \omega_e = \omega_s b^{\frac{1}{2}},$$

where $b = \sin(\theta_B - \alpha) / \sin(\theta_B + \alpha)$. The beamwidth changes proportionally with b . This latter property of asymmetric–symmetric monochromators is of particular interest where a demagnified image of the primary source is required (e.g. powder diffraction and small angle scattering). Note, however, that one no longer has a truly tunable monochromator system.

(e) X-ray Powder Diffraction

Having conditioned the incident beam to the appropriate size and wavelength one can place in position a conventional vertical powder diffractometer with all of its attachments. These can include a specimen spinning stage (necessary because the collimation of the incident beam is such that spinning or rocking of the specimen is necessary to bring sufficient particles into the diffracting condition), diffracted beam monochromators, and detectors (usually scintillation or proportional detectors) with their associated pulse height analysis and pulse counting modules.

A number of descriptions of the use of conventional powder diffraction techniques in conjunction with synchrotron radiation sources have been published recently (Skelton 1984; Parrish and Hart 1985; Suortti *et al.* 1985; Sabine 1987). The system described in the latter two papers comprises a channel-cut (grooved) monochromator of silicon, a sample and a diffracted beam monochromator with the choice of cut for the monochromators adjusted to optimise the system resolution. Parrish and Hart (1985) did not use a diffracted beam monochromator but relied on soller slits to adjust the diffracted beam geometry.

Suortti *et al.* (1985) used a variety of configurations of monochromator: Si(220) channel cut for the incident beam, Ge(111) for the diffracted beam; Ge(111) for the incident beam, Ge(440) for the diffracted beam; Ge(111) for the incident beam, Ge(220) for the diffracted beam. The resolution achieved was at best 0.02° FWHM at $2\theta = 60^\circ$. The instrument resolution function was a roughly parabolic function of the diffracted beam (2θ) angle. In contrast, the Parrish–Hart (1985) system produced

a resolution function which was almost independent of diffracted beam angle. The resolution of their instrument remained constant at 0.19° for a diffracted beam range 20° – 140° .

Sabine (1987) has described the design features of an instrument, yet to be built, for which the resolution is claimed to be superior to all previously built instruments. However, the resolution function is predicted to be strongly dependent on diffracted beam angle. All of these diffractometers have resolutions which are almost an order of magnitude better than those used with conventional laboratory sources.

Because X-ray powder diffractometer systems must satisfy a wide range of performance criteria it is necessary that these systems be triple-axis systems. The most important component of such a system is the incident beam monochromator since this element converts the initially linearly polarised white radiation into a form suitable for use in the chosen experiment.

The monochromator (Fig. 5) proposed at the Photon Factory, Tsukuba, Japan will be housed in a casting capable of evacuation. Within this housing a number of monochromator devices will be available. The detailed design of these monochromators depends on the type of beam line to which they are mated. Different monochromator characteristics are necessary if the beam line contains a wiggler, an undulator, or totally reflecting mirrors.

The most commonly used monochromator is usually a symmetrically reflecting double crystal diffracting in the vertical plane. Provision will be made for the easy interchange of monochromator crystals, a choice being given of Si(111) or Ge(111) monochromator crystals.

For experiments in which the beam dimension needs to be changed, a separate monochromator will be moved into the beam in place of the symmetrical double crystal monochromator. This monochromator will be fabricated from single crystal

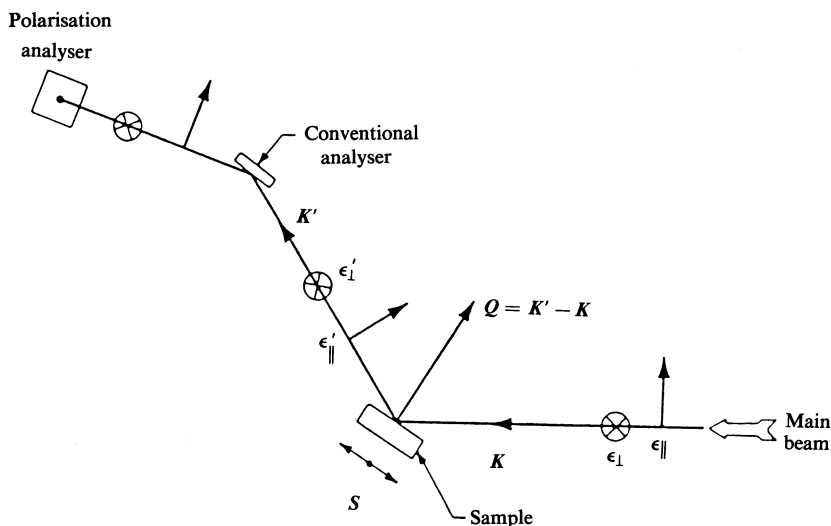


Fig. 6. Schematic representation of the magnetic scattering geometry used for holmium. The orientations of the incident and scattered photon wave vectors and polarisations are shown as well as the orientation of the sample and the spin direction. The orientation is shown of a polarisation analyser assembly which passes only the ϵ'_{\perp} scattered component since it reflects radiation 90° out of the plane of the diagram.

silicon so as to produce an asymmetric-symmetric pair of Bragg reflections. The angle of cut of the asymmetric surface relative to the Bragg plane will depend on the amount of demagnification required. Because these devices operate in a fixed wavelength range several interchangeable grooved crystals will be required. Probable wavelengths to be offered will encompass the characteristic K-shell emission lines of molybdenum, copper, cobalt and chromium.

Another monochromator to be housed in the vacuum vessel will be a high resolution device comprised of two symmetrically cut silicon (111) grooved crystal monochromators, rotated in opposite senses so as to maintain the Bragg condition at both crystals, and to keep the exit beam position constant. These grooved crystals may be either of the type described by Hart *et al.* (1984) or a simple grooved crystal configuration.

If magnetic scattering experiments are to be undertaken then a special monochromator will be required to convert the linearly polarised incident beam into a circularly polarised exit beam. This can be done by replacing one of the reflecting surfaces of one of the grooved crystal monochromator elements by a dynamically diffracting parallel-sided perfect crystal plate. Its thickness is chosen so as to produce a $\lambda/4$ path difference between the σ and π components of the wavefield at the chosen wavelength of operation λ .

5. Diffraction Studies of Holmium using High Resolution Powder Diffraction

Here I will illustrate the use of high resolution powder diffractometer measurements which may be performed at a synchrotron radiation source with reference to experiments on magnetic scattering of photons from a holmium single crystal specimen.

The interaction cross sections for magnetic scattering from condensed matter were first investigated theoretically by Platzman and Tzoar (1970) and observed by de Bergevin and Brunel (1972). Fig. 6 shows schematically the scattering geometry used to investigate magnetic scattering. The configuration is that of a high resolution powder diffractometer. It shows the orientations of the incident and scattered photon wave vectors and polarisation as well as the orientation of the sample and the spin direction. Included is a polarisation analyser which is set to scatter only the component of the scattered electric vector parallel to the plane of the orbit into the detector.

The initial states of the photon and the sample are respectively $(k, \epsilon, \lambda, \omega)$ and $|a\rangle$, and the final states are $(k', \epsilon', \lambda', \omega')$ and $|b\rangle$. The differential scattering cross section can then be written as

$$\left(\frac{d^2\sigma}{dE' d\Omega'}\right)_{k,\epsilon \rightarrow k',\epsilon'}^{a \rightarrow b} = \left(\frac{e^2}{mc^2}\right)^2 \left(\langle b | \sum_j e^{iQ \cdot r_j} | a \rangle \epsilon' \cdot \epsilon \right)^2 \delta(E_a - E_b + \hbar\omega - \hbar\omega') \\ - \frac{i\hbar\omega}{mc^2} \langle b | \sum_j e^{iQ \cdot r_j} \left(\frac{iQ \times P_j}{\hbar k^2} \cdot A + S_j \cdot B \right) | a \rangle. \quad (2)$$

The photon has the transferred momentum

$$\hbar Q = \hbar k' - \hbar k$$

and the sums are taken over all electrons including their positions, momenta and spins represented by r_j , P_j and S_j respectively. The polarisation states are chosen either parallel or perpendicular to the scattering plane (that plane which contains the propagation vectors k and k'). The vectors A and B are

$$A = \begin{matrix} \epsilon_1 & \epsilon_{\parallel} \\ \epsilon'_1 & 0 & -\hat{k} \\ \epsilon'_{\parallel} & \hat{k}' & \hat{k}' \times \hat{k} \end{matrix} \quad B = \begin{matrix} \epsilon_1 & \epsilon_{\parallel} \\ \epsilon'_1 & \hat{k} \times \hat{k}' & -2\hat{k}' \sin^2 \theta \\ \epsilon'_{\parallel} & 2\hat{k} \sin^2 \theta & \hat{k} \times \hat{k}' \end{matrix}$$

Using the same formalism the polarisation dependence $\epsilon' \cdot \epsilon$ for the Thomson scattering term can be written as

$$\epsilon' \cdot \epsilon = \begin{matrix} \epsilon_1 & \epsilon_{\parallel} \\ \epsilon'_1 & 1 & 0 \\ \epsilon'_{\parallel} & 0 & \cos 2\theta \end{matrix}$$

Pure magnetic scattering is contained in the imaginary term in equation (2). For anti-ferromagnets this term produces scattering at reciprocal lattice points separate from the main Bragg peaks, and the amplitude of the purely magnetic scattering cross section is about 2% of that for the Coulomb (Thomson) scattering cross section which gives rise to the principal diffraction peaks. The magnetic form factor is, however, more sensitive to variations in Q than the atomic form factor. We may write the ratio of the magnetic scattering cross section to the charge scattering cross section as

$$\sigma_m / \sigma_c = (\hbar\omega / mc^2)^2 (N_m^2 / N) \langle S \rangle^2 (f_m / f)^2.$$

Here N_m is the number density of magnetic scattering electrons in an ensemble containing an electron number density N .

The fact that the magnetic term is imaginary leads to interference effects which may be of importance in crystal systems for which the magnetic and crystal structures both have significant scattering at the same wave vectors. This situation occurs in ferromagnets, ferrimagnets and commensurate anti-ferromagnets.

Experimental configurations are devised to enable the incident photons in an ϵ_1 state to interact with a spin S in the sample oriented normal to the scattering plane. The magnetic term in the expression for the differential scattering cross section becomes

$$(i\hbar\omega / mc^2) \langle \sum_j e^{iQ \cdot r_j} S_{Nj} \sin 2\theta \rangle,$$

where S_N is the component of S along $\hat{k} \times \hat{k}'$. In the neighbourhood of an absorption edge the imaginary part of the form factor f_j'' may increase significantly causing a change in the scattered intensity:

$$\Delta I / I = (4\hbar\omega / mc^2) (f'')^2 S_N \sin 2\theta / (f'^2 + f''^2).$$

Magnetic scattering effects are enhanced near the edge. The geometry chosen for this experiment eliminates the effect of orbital magnetisation since the matrix element for A vanishes.

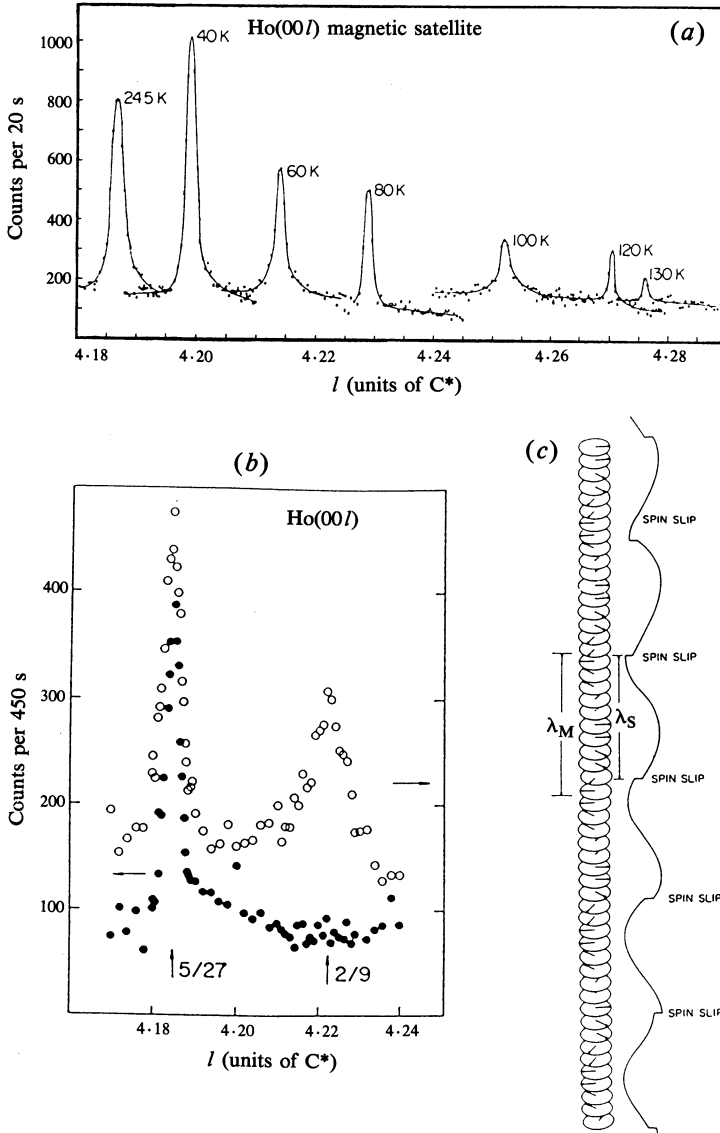


Fig. 7. (a) Temperature dependence of the $Ho(004)^+$ magnetic satellite taken with synchrotron radiation (with lines drawn to guide the eye). [From Moncton *et al.* (1986).] (b) Open circles give the scan of the $Ho(004)$ magnetic ($\tau_m = 5/27$) and charge ($\tau_c = 2/9$) satellites taken at 17 K. Closed circles are for the same scan, but with the polarisation analyser in place. (c) Idealised model of the magnetic structure of holmium in the $5/27$ state. Note the periodic arrangement of spin slips every nine layers; thus $\lambda_S = \lambda_M = 54/5 = 10.8$.

Holmium metal has a dhcp structure. Below $T_N = 131$ K and above $T_C = 20$ K spiral magnetisation waves develop. This structure consists of uniformly magnetised layers with the direction of magnetisation rotating as the position on the c -axis

is changed. It is possible to describe this in terms of a wavelength λ_N which is temperature dependent, varying from ~ 7 layers at the Néel point (131 K) to ~ 11 layers at 24 K. Satellite magnetic Bragg reflections occur at

$$Q = Q_{hkl} + \tau,$$

where Q_{hkl} defines the main Bragg reflection and $\tau = (0, 0, 2/\lambda_M)$. The factor 2 arises because there are two layers per chemical unit cell. The strongest magnetic Bragg reflections are those for which $Q = (0, 0, l \pm 2/\lambda_M)$ where l is even. Fig. 7a shows the development of the magnetic satellite for $(0, 0, l)$ as the temperature is varied. That the use of the polarisation analyser enhances the ability to distinguish between magnetic ($\tau_m = 5/27$) and charge ($\tau_c = 2/9$) satellites at 17 K is readily seen in Fig. 7b.

Moncton *et al.* (1986) interpreted the data from their study of a single crystal holmium crystal by invoking the concept of spin slips. Fig. 7c shows schematically a $5/27$ structure. In this model the spins align themselves in pairs along the direction of easy magnetisation—the basal plane, along the hexagonal a axes or along the mirror planes bisecting them. The spin pairs normally rotate 60° per double layer. Their model then introduces a spin slip, the equivalent of a phase shift of 60° at regular positions along the c -axis. There are five spin slips for the 27 dhcp layers (or 64 close packed layers). The peak observed in their data at $2/9$ is thought to result from diffraction from the spin slips due to magnetoelastic couples.

In a more recent paper (Bohr *et al.* 1986) the concept of spin slips was developed further to give a phenomenological model for one-dimensional spatially propagating magnetic structures. It must be stressed, however, that the authors gave no indication as to what they considered to be the origin of the spin slips. Indeed, their initial belief was that the magnetic lattice was incommensurate with the crystal lattice. It would seem likely however that the spin slips have their origin in the existence of ordered arrays of stacking faults in the dhcp crystal structure. As mentioned earlier a stacking fault in a dhcp structure is equivalent to the insertion of a region of cubic symmetry into the structure. Thus the perfect layer stacking, which may be alternatively characterised according to whether a particular site is spanned by like h , corresponding to the hcp structure, or dissimilar lattice sites c , corresponding to the fcc structure, may be written for holmium as

... ABACABACABABAC

... c h c h c h c h c h c h c h ...

Atoms in a cubic environment are acted on by a crystal field which tends to suppress the ordering of magnetic moments, whereas those in a hcp environment can undergo ordering. Achiwa and Kawano (1985) have observed this type of behaviour in terbium–light rare earth alloys which have the samarium structure.

Thus, in the dhcp structure the spin spiral advances along the c -axis with spin moments only on those planes for which the atoms are in a hcp environment; i.e. the spin advances by 60° every unit cell of the dhcp crystal, the easy axes being determined either by the hexagonal (rhombohedral) axes or axes bisecting them at 30° .

The introduction of a stacking fault into the perfect crystal array changes the sequence of the spins. Thus, the sequence becomes that shown in Fig. 8.

The slip of lattice planes induces a jog in the spin wave. Techniques exist for the analysis of such spin structures (Kakinoki and Komura 1965). They are akin to stacking faults in the real crystal lattice and may be described in terms of the stacking fault probabilities α and β .

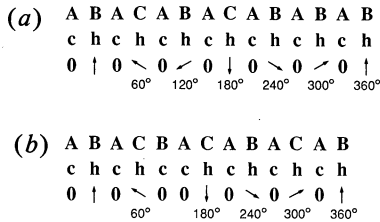


Fig. 8. Spin spiral rotation in (a) a perfect dhcp lattice and (b) a faulted dhcp lattice.

For a perfect crystal the spin lattice would produce magnetic scattering reciprocal lattice points related to the phase advance angle of the spiral. If this is 60° then the repetition period is six hexagonal unit cells, or twelve close packed layers. If, however, stacking faults are present the faulting of the spin spiral wave will cause destructive (or constructive) interference between both waves in the perfect and in the faulted material. This substantially affects the location, intensity, and integral breadth of the magnetic reflections. Since the probability of martensitic transformation is high there is likely to be a strong decrease of magnetically scattered intensity and deviation from the true reciprocal lattice position with temperature. That this is the case for holmium can be seen clearly in Fig. 7a.

It should also be stressed that the technique used to detect the magnetic scattering is a powder diffraction technique and therefore the analysis of the data yields only the probability of formation of stacking faults. Given the data in Fig. 7a it is likely that there is a regular variation in the stacking fault probabilities α and β over the temperature range, the major variation being in the growth fault probability α .

It may be concluded therefore that the spin slip model proposed by Bohr *et al.* (1986) is related to the model based on stacking fault formation but lacks its generality and sophistication. Nevertheless, their study is the first systematic study of magnetic scattering by ordered materials. Another comment which may be made concerns their experimental apparatus. Although magnetic scattering experiments are best performed using circularly polarised incident radiation, a simple modification to the high resolution monochromator through the insertion of a dynamically diffracting Laue-case element would enable the provision of such a circularly polarised beam. A schematic diagram of such a device, planned for the Tsukuba experimental station, is shown in Fig. 5. Further, the simple nature of the polarisation analyser used by Moncton *et al.* (1986) limited the energy of the incident photons to the fixed value 7.8 keV. The inclusion of such devices would enable the experiment to be performed at photon energies in the neighbourhood of the holmium L-absorption edge where enhancement of the magnetic-to-charge scattering cross section will occur (Brunel *et al.* 1983).

6. Conclusions

It has been shown that, by using a variety of experimental techniques available at synchrotron radiation facilities, it is possible to establish a link between the structural and magnetic properties of the light rare earth elements and their alloys. It has also been shown that the concept of magnetic stacking faults introduced by Kakinoki and Komura (1965) can be applied to data gained from magnetic scattering experiments. Few experiments of this type have been undertaken so far and much more has to be done if the relation between structural and magnetic properties is to be established beyond doubt.

References

- Achiwa, N., and Kawano, S. (1985). *J. Magnetism Magn. Mater.* **52**, 461–3.
- Bertin, E. P. (1975). 'Principles and Practice of X-ray Spectrometric Analysis' (Plenum: New York).
- Bianconi, A., Incoccia, L., and Stipich, S. (Eds) (1983). 'EXAFS and Near Edge Structure' (Springer: Berlin).
- Bohr, J., Gibbs, D., Moncton, D. C., and D'Amico, K. L. (1986). *Physica A* **140**, 349–58.
- Bonse, U., and Hart, M. (1965). *Appl. Phys. Lett.* **7**, 238–40.
- Brunel, P. M., Patrat, G., de Bergevin, F., Rousseau, F., and Lemmonnier, M. (1983). *Acta Crystallogr. A* **39**, 84.
- Chikawa, J., Sato, F., Kawamura, T., Yamahita, T., and Croto, W. (1986). In 'X-ray Instrumentation for the Photon Factory' (Eds S. Hosoya *et al.*), pp. 14–57 (KTK: Tokyo).
- Clark, G. E., and Tanner, B. K. (1980). *Phys. Status Solidi (a)* **59**, 241–9.
- Coles, B. R. (1980). In 'Proc. Int. Conf. on Magnetism' (Eds W. Ziner *et al.*), pp. 1225–6 (North Holland: Amsterdam).
- Creagh, D. (1985). Comments on paper by Moncton *et al.* at Int. Workshop on X-ray Scattering, Asilomar (Eds R. Pratt and N. del Grande), p. 23 (Lawrence Livermore Laboratory).
- Creagh, D. C., and Ayling, S. (1978). *J. Mater. Sci.* **13**, 113–22; 2723–5.
- Creagh, D. C., Bailey, S. G., and Wilson, G. V. H. (1975). *Philos. Mag.* **32**, 405–15.
- de Bergevin, F., and Brunel, M. (1972). *Phys. Rev. Lett.* **39**, 141–3.
- Egami, T. (1978). *J. Mater. Sci.* **13**, 2587–99.
- Hart, M., and Rodrigues, A. R. D. (1978). *J. Appl. Crystallogr.* **11**, 245–53.
- Hart, M., and Rodrigues, A. R. D. (1979). *Philos. Mag. B* **40**, 149–57.
- Hart, M., Rodrigues, A. R. D., and Siddons, D. P. (1984). *Acta Crystallogr. A* **40**, 502–7.
- Hashizume, H., and Kohra, K. (1971). *J. Phys. Soc. Jpn* **31**, 204–16.
- Hosoya, S., Iitaka, Y., and Hashizume, H. (1986). 'X-ray Instrumentation for the Photon Factory' (KTK: Tokyo).
- Kakinoki, J., and Komura, Y. (1965). *Acta Crystallogr.* **19**, 137.
- Kikuta, K., and Kohra, K. (1968). *Acta Crystallogr. A* **24**, 200–5.
- Kikuta, K., and Kohra, K. (1970). *J. Phys. Soc. Jpn* **29**, 1322–8.
- Lang, A. R. (1959). *Acta Crystallogr.* **12**, 249–61.
- McKenna, T. J., Campbell, S. J., Chaplin, D. H., and Wilson, G. V. H. (1980). *J. Magnetism Magn. Mater.* **15–18**, 1497–8.
- Matsushita, T., Kikuta, S., and Kohra, K. (1971). *J. Phys. Soc. Jpn* **30**, 1136–44.
- Miltat, J. (1978). *Nucl. Instrum. Methods* **152**, 323–9.
- Moncton, D. E., Gibbs, D., and Bohr, J. (1986). *Nucl. Instrum. Methods A* **246**, 839–44.
- Parrish, W., and Hart, M. (1985). *Trans. Am. Crystallogr. Assoc.* **21**, 51–5.
- Platzman, P. M., and Tzoar, N. (1970). *Phys. Rev. B* **2**, 3556–9.
- Renniger, M. (1967). *Adv. X-ray Anal.* **10**, 32–39.
- Sabine, T. (1987). *J. Appl. Crystallogr.* **30**, 173–9.
- Skelton, E. F. (1984). *Phys. Today* **37** (Sept.), 44–62.
- Suortti, P., Hastings, J. B., and Cox, D. E. (1985). *Acta Crystallogr. A* **41**, 413–7.

- Tanner, B. K. (1977). *Prog. Cryst. Growth Charact.* **1**, 29–56.
- Teo, B. K., and Joy, D. C. (Eds) (1981). 'EXAFS Spectroscopy' (Plenum: New York).
- Van Vucht, J. H. N., and Buschow, K. H. J. (1965). *J. Less Common Metals* **19**, 98–108.
- Warren, B. E. (1969). 'X-ray Diffraction' (Addison-Wesley: London).

Manuscript received 21 August, accepted 29 September 1987